Verilog-A behavioral model for resonance-modulated silicon micro-ring modulator

Jinsoo Rhim, Yoojin Ban, Byung-Min Yu, Jeong-Min Lee, and Woo-Young Choi*

Department of Electrical and Electronic Engineering, Yonsei University, 50 Yonsei-ro, Seodaemun-gu, Seoul, South Korea

*wchoi@yonsei.ac.kr

Abstract: We present an accurate behavior model for Si micro-ring modulators (MRM) based on Verilog-A, a standard simulation tool for electronic system design. Our model describes the electrical characteristics of the Si MRM using an equivalent circuit and the optical characteristics based on the couple-mode theory. The accuracy of our model is confirmed by comparing simulation results of our behavior model with the measurement results of a fabricated Si MRM. With this behavior model, co-simulation of Si MRM and electronic driving circuits in the standard electronic design environment can be easily performed.

OCIS codes: (130.3120) Integrated optics devices; (130.4110) Modulators; (250.0250) Optoelectronics; (230.5750) Resonators; (040.6040) Silicon; (250.7360) Waveguide modulators.

References and links

1. I. A. Young, E. Mohammed, J. T. S. Liao, A. M. Kern, S. Palermo, B. A. Block, M. R. Reshotko, and P. L. D. Chang, "Optical I/O technology for tera-scale computing," IEEE J. Solid-State Circuits **45**(1), 235–248 (2010).
2. M. A. Taubenblatt, "Optical interconnects for high-performance computing," IEEE/OSA J. Lightwave Technol. **30**(4), 448–457 (2012).
3. X. Zheng, D. Patil, J. Lexau, F. Liu, G. Li, H. Thacker, Y. Luo, I. Shubin, J. Li, J. Yao, P. Dong, D. Feng, M. Asghari, T. Pinguet, A. Mekis, P. Amberg, M. Dayringer, J. Gainsley, H. F. Moghadam, E. Alon, K. Raj, R. Ho, J. E. Cunningham, and A. V. Krishnamoorthy, "Ultra-efficient 10 Gb/s hybrid integrated silicon photonic transmitter and receiver," Opt. Express **19**(6), 5172–5186 (2011).
4. G. Kim, J. W. Park, I. G. Kim, S. Kim, S. Kim, J. M. Lee, G. S. Park, J. Joo, K.-S. Jang, J. H. Oh, S. A. Kim, J. H. Kim, J. Y. Lee, J. M. Park, D.-W. Kim, D.-K. Jeong, M.-S. Hwang, J.-K. Kim, K.-S. Park, H.-K. Chi, H.-C. Kim, D.-W. Kim, and M. H. Cho, "Low-voltage high-performance silicon photonic devices and photonic integrated circuits operating up to 30 Gb/s," Opt. Express **19**(27), 26936–26947 (2011).
5. J. F. Buckwalter, X. Zheng, G. Li, K. Raj, and A. V. Krishnamoorthy, "A monolithic 25-Gb/s transceiver with photonic ring modulators and Ge detectors in a 130-nm CMOS SOI process," IEEE J. Solid-State Circuits **47**(6), 1309–1322 (2012).
6. L. Zimmermann, D. J. Thomson, B. Goll, D. Knoll, S. Lischke, F. Y. Gardes, Y. Hu, G. T. Reed, H. Zimmermann, and H. Porte, "Monolithically integrated 10Gbit/sec Silicon modulator with driver in 0.25µm SiGe:C BiCMOS," in *Proceedings of European Conference on Optical Communication (ECOC)*, pp. 1–3 (2013).
7. J.-S. Youn, M.-J. Lee, K.-Y. Park, H. Rücker, and W.-Y. Choi, "An integrated 12.5-Gb/s optoelectronic receiver with a silicon avalanche photodetector in standard SiGe BiCMOS technology," Opt. Express **20**(27), 28153–28162 (2012).
8. T. Smy, P. Gunupudi, S. Mcgarry, and W. N. Ye, "Circuit-level transient simulation of configurable ring resonators using physical models," J. Opt. Soc. Am. B **28**(6), 1534–1543 (2011).
9. W. Bogaerts, M. Fiers, and P. Dumon, "Design challenges in silicon photonics," IEEE J. Sel. Top. Quantum Electron. **20**(4), 8202008 (2014).
10. L. Chrostowski, J. Flueckiger, C. Lin, M. Hochberg, J. Pond, J. Klein, J. Ferguson, and C. Cone, "Design methodologies for silicon photonic integrated circuits," Proc. SPIE **8989**, 89890G (2014).
11. K. Zhu, V. Saxena, and W. Kuang, "Compact Verilog-A modeling of silicon traveling-wave modulator for hybrid CMOS photonic circuit design," in *Proceedings of IEEE International Midwest Symposium on Circuits and Systems*, pp. 615–618 (2014).
12. D. J. Thomson, F. Y. Gardes, J.-M. Fedeli, S. Zlatanovic, Y. Hu, B. P. P. Kuo, E. Myslivets, N. Alic, S. Radic, G. Z. Mashanovich, and G. T. Reed, "50-Gb/s silicon optical modulator," IEEE Photon. Technol. Lett. **24**(4), 234–236 (2012).

#231700 - $15.00 USD Received 30 Dec 2014; revised 4 Mar 2015; accepted 18 Mar 2015; published 30 Mar 2015

13. X. Zheng, F. Y. Liu, J. Lexau, D. Patil, G. Li, Y. Luo, H. D. Thacker, I. Shubin, J. Yao, K. Raj, R. Ho, J. E. Cunningham, and A. V. Krishnamoorthy, "Ultralow power 80 Gb/s arrayed CMOS silicon photonic transceivers for WDM optical links" IEEE/OSA J. Lightwave Technol. **30**(4), 641–650 (2012).
14. J. Rhim, Y. Ban, J.-M. Lee, S.-H. Cho, and W.-Y. Choi, "A behavior model for silicon micro-ring modulators and transmitter circuit-level simulation using it," in *Proceedings of IEEE International Conference on Group IV Photonics*, pp. 7–8 (2014).
15. B. E. Little, S. T. Chu, H. A. Haus, J. Foresi, and J.-P. Laine, "Microring resonator channel dropping filters" J. Lightwave Technol. **15**(6), 998–1005 (1997).
16. L. Zhang, Y. Li, J.-Y. Yang, M. Song, R. G. Beausoleil, and A. E. Willner, "Silicon-based microring resonator modulators for intensity modulation," IEEE J. Sel. Top. Quantum Electron. **16**(1), 149–158 (2010).
17. B.-M. Yu, J.-M. Lee, Y. Ban, S.-H. Cho, and W.-Y. Choi, "Model parameter extraction for Si micro-ring modulators," presented at OptoElectronics and Communication Conference and the Australian Conference on Optical Fibre Technology (OECC/ACOFT), Melbourne, Australia, 6–10 July, 2014.
18. X. Zheng, Y. Luo, G. Li, I. Shubin, H. Thacker, J. Yao, K. Raj, J. E. Cunningham, and A. V. Krishnamoorthy, "Enhanced optical bistability from self-heating due to free carrier absorption in substrate removed silicon ring modulators," Opt. Express **20**(10), 11478–11486 (2012).
19. W. D. Sacher, W. M. J. Green, S. Assefa, T. Barwicz, H. Pan, S. M. Shank, Y. A. Vlasov, and J. K. S. Poon, "Coupling modulation of microrings at rates beyond the linewidth limit," Opt. Express **21**(8), 9722–9733 (2013).
20. J. Müller, F. Merget, S. S. Azadeh, J. Hauck, S. R. García, B. Shen, and J. Witzens, "Optical peaking enhancement in high-speed ring modulators," Sci. Rep. **4**, 6310 (2014).
21. Y. Ban, J.-M. Lee, B.-M. Yu, S.-H. Cho, and W.-Y. Choi, "Small-signal frequency responses for Si micro-ring modulators," in *Proceedings of IEEE Optical Interconnects Conference*, pp. 47–48 (2014).

1. Introduction

There are growing interests in optical interconnects as they can provide higher bandwidth and more energy-efficient solutions to many interconnect applications than is possible with electrical interconnects [1,2]. In particular, Si photonics is very attractive for optical interconnect applications as it is capable of providing high-performance integrated photonic devices in a cost-effective manner [3,4]. Furthermore, with Si photonics, it is possible to integrate photonic devices and Si electronics on the same Si platform, with which new and more powerful integrated solutions can be realized than is possible with photonics or electronics alone. Several such electronic-photonic integrated circuits (EPICs) have been reported [5–7].

For successful realization of EPICs, it is very important to be able to co-simulate photonic devices and electronic circuits on a single simulation platform in the initial design stage. Such co-simulation can be challenging as simulation techniques for photonics and electronics are usually based on completely different platforms and, consequently, not easily compatible with each other. For this reason, there are growing research interests in developing simulation techniques that can handle both photonic devices and electronic circuits [8–11].

We present a simple and easy-to-use co-simulation method that can be used for EPIC design. In particular, we take an approach in which behavior models for photonic devices are implemented in Verilog-A. Verilog is a popular hardware description language used for high-level behavioral description of electronic systems, and Verilog-A is an extended version of Verilog that supports analog signals. The characteristics of any photonic component can be modeled in the behavior level as long as the values of model parameters can be accurately determined. Although there are many different methods for implementing such behavior models, our approach based on Verilog-A is particularly useful for EPIC applications since Verilog-A behavior models can be easily co-simulated with any electronic circuits in the standard electronic design environment. Establishing such compatibility is very important in order to successfully introduce Si photonic devices into the Si electronics world.

The photonic device of our interest is depletion-type Si micro-ring modulators (MRMs), which are expected to play an important role for high-speed small-footprint optical interconnect systems [12]. Si MRMs can provide very large modulation bandwidth with much smaller footprint and are capable of wavelength division multiplexing (WDM) [13].

This paper is organized as follows. In chapter 2, we give a brief introduction of the Si MRM modulator and describe its electrical and optical characterizations, from which our

#231700 - $15.00 USD Received 30 Dec 2014; revised 4 Mar 2015; accepted 18 Mar 2015; published 30 Mar 2015

Verilog-A behavior model is developed. In chapter 3, we verify the accuracy of our behavioral model by comparing model simulation results with measurement results of a fabricated Si MRM. Finally, we conclude this paper in chapter 4. A very brief version of this paper has been reported in [14].

2. Modeling a Si micro-ring modulator

Figure 1 shows the structure of a Si MRM. In this work, we focus on a resonance-modulated depletion-type Si MRM. It consists of ring and bus waveguides, which are located close to each other forming a directional coupler. About three quarters of the ring waveguide are doped to form a lateral PN junction so that its effective group index can be modulated by the reverse-bias voltage applied to the PN junction.

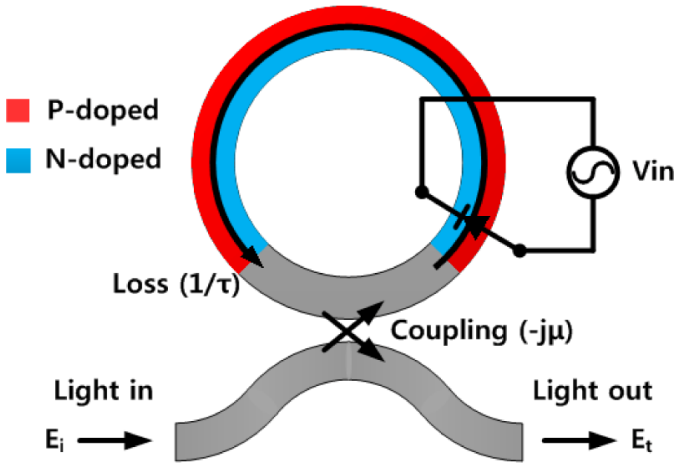

Fig. 1. Structure of Si MRM.

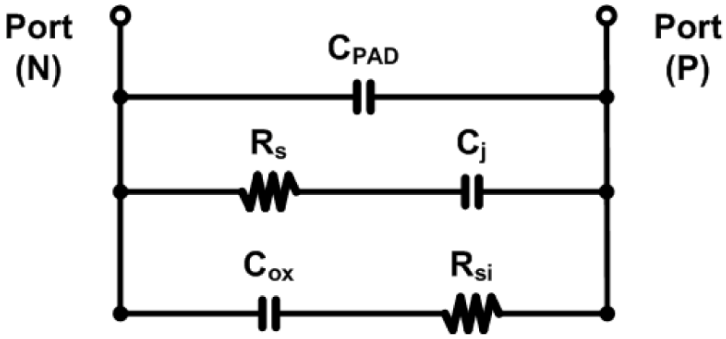

Fig. 2. Equivalent circuit model for Si MRM.

Si MRMs have both electrical and optical characteristics, which should be modeled separately. For the electrical characteristics, an equivalent circuit model based on passive electrical components can be used [3]. Figure 2 shows the equivalent circuit model where C_{ox}, C_j, R_s, and R_{si} represent capacitance through the buried oxide layer, of the depletion region in PN junction, diode series resistance, and resistance through the Si substrate, respectively. C_{PAD} represents the parasitic capacitance of the signal pad used for measurement.

For optical characteristics of resonance-modulated Si MRM, a model based on the coupled-mode theory can be used, which describes the rate of change in time for the energy amplitude, *a(t)*, inside the ring in the following manner [15,16],

#231700 - $15.00 USD Received 30 Dec 2014; revised 4 Mar 2015; accepted 18 Mar 2015; published 30 Mar 2015

$$\frac{d}{dt}a(t)=\left(j\omega_r-\frac{1}{\tau}\right)a(t)-j\mu E_i(t). \tag{1}$$

Here, $E_i(t)$ is the incident optical field in the bus waveguide, ω_r is the ring resonance angular frequency given as $\omega_r=\frac{2\pi mc}{\eta_{eff}L}$, where m is an integer representing the mode number, η_{eff} is the effective index for the ring waveguide, and L is the circumference of the ring. τ is decay time constant given as $\frac{1}{\tau}=\frac{1}{\tau_l}+\frac{1}{\tau_e}$, where τ_l and τ_e are the decay time constants due to the round-trip loss and ring-bus coupling, respectively. μ is the mutual coupling coefficient between the ring and the bus and related to τ_e by $\mu^2=\frac{2}{\tau_e}$. The output optical field, $E_t(t)$, is given as

$$E_t(t)=E_i(t)-j\mu a(t). \tag{2}$$

When the MRM is electrically modulated by $v(t)$, the values of such parameters as η_{eff}, τ_l, and τ_e change with the applied voltage, and $a(t)$ as well as $E_t(t)$ change dynamically according to Eq. (1) and Eq. (2). In order to model such dynamics, it is necessary to solve the differential equation given in Eq. (1) numerically in an efficient manner. The solution for Eq. (1) with the incident optical field $E_i(t)=E_0\exp(j\omega t)$ is the sum of the homogeneous and the steady-state solutions, or

$$a(t)=P\exp\left(j\omega_r t-\frac{1}{\tau}t\right)+Q\exp(j\omega t), \tag{3}$$

where P and Q are, respectively, the homogeneous and steady-state coefficients that need to be determined. For numerical solutions, $v(t)$ can be approximated with the series of constant values shown in Fig. 3 assuming the time step is sufficiently small, or

$$v(t)\cong\begin{cases} v_0=v(t_0), & t_0\le t<t_1 \\ v_1=v(t_1), & t_1\le t<t_2 \\ \vdots & \vdots \\ v_k=v(t_k), & t_k\le t<t_{k+1} \end{cases}. \tag{4}$$

Then, corresponding $a(t)$ can be represented as

$$a(t)=\begin{cases} a_0(t)=P_0\exp\left(j\omega_{r,0}t-\frac{1}{\tau_0}t\right)+Q_0\exp(j\omega t), & t_0\le t<t_1 \\ a_1(t)=P_1\exp\left(j\omega_{r,1}t-\frac{1}{\tau_1}t\right)+Q_1\exp(j\omega t), & t_1\le t<t_2 \\ \vdots & \vdots \\ a_k(t)=P_k\exp\left(j\omega_{r,k}t-\frac{1}{\tau_k}t\right)+Q_k\exp(j\omega t), & t_k\le t<t_{k+1} \end{cases}, \tag{5}$$

where P_k and Q_k are the homogeneous and steady-state coefficients, and $\omega_{r,k}$ and τ_k are the optical parameter, all of which are influenced by v_k when $t_k\le t<t_{k+1}$.

#231700 - $15.00 USD Received 30 Dec 2014; revised 4 Mar 2015; accepted 18 Mar 2015; published 30 Mar 2015

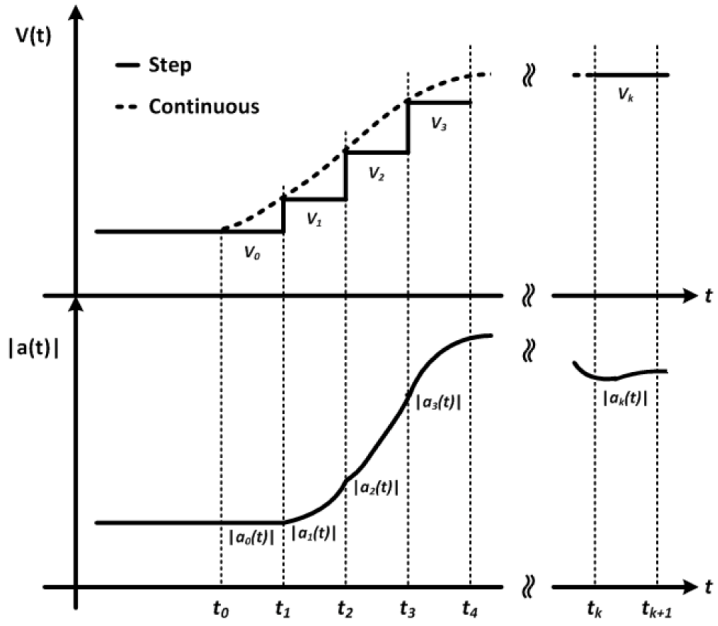

Fig. 3. Step change in the modulation voltage and numerical calculation of a(t).

Since the energy in the ring should be continuous at each boundary of time steps, $a_{k-1}(t_k)$ should be equal to $a_k(t_k)$. Assuming $a(t_0)$ has reached the steady-state, we can set $P_0 = 0$ and $a_0(t) = Q_0 \exp(j\omega t)$. Q_0 can be determined by substituting $a_0(t)$ into Eq. (1) as

$$Q_0 = \frac{-j\sqrt{\frac{2}{\tau_{e,0}}}}{j(\omega - \omega_{r,0}) + \frac{1}{\tau_0}} E_0. \tag{6}$$

$a_1(t)$ can be determined if P_1 and Q_1 are known. Since Q_1 is the steady-state coefficient, it should have the same expression as in Eq. (6) with corresponding values for τ_e, τ, and ω_r. P_1 can be evaluated at $t = t_1$ from Eq. (3) as

$$P_1 = \left[a_0(t_1) - Q_1 \exp(j\omega t_1)\right] \exp\left(-j\omega_{r,1} t_1 + \frac{1}{\tau_1} t_1\right), \tag{7}$$

where $a_1(t_1) = a_0(t_1)$ is used. Above process can be repeated for higher values of index k, and we have following iterative equations:

$$P_k = \left[a_{k-1}(t_k) - Q_k \exp(j\omega t_k)\right] \exp\left(-j\omega_{r,k} t_k + \frac{1}{\tau_k} t_k\right). \tag{8}$$

$$Q_k = \frac{-j\sqrt{\frac{2}{\tau_{e,k}}}}{j(\omega - \omega_{r,k}) + \frac{1}{\tau_k}} E_0. \tag{9}$$

#231700 - $15.00 USD Received 30 Dec 2014; revised 4 Mar 2015; accepted 18 Mar 2015; published 30 Mar 2015

$$
\begin{aligned}
a_k(t) &= P_k \exp\left(j\omega_{r,k} t - \frac{1}{\tau_k} t \right) + Q_k \exp\left(j\omega t \right) \\
&= \left[a_{k-1}(t_k) - Q_k \exp\left(j\omega t_k \right) \right] \exp\left[\left(j\omega_{r,k} - \frac{1}{\tau_k} \right) \left(t - t_k \right) \right] + Q_k \exp\left(j\omega t \right).
\end{aligned} \tag{10}
$$

When the time step, Δt, is very small, $a_k(t)$ for $t_{k-1} \le t < t_k$ can be approximated by a constant value, A_k, or

$$
\begin{aligned}
A_k &= a_k(t_k) = a_{k-1}(t_k) \\
&= \left[a_{k-2}(t_{k-1}) - Q_{k-1} \exp\left(j\omega t_{k-1} \right) \right] \exp\left[\left(j\omega_{r,k-1} - \frac{1}{\tau_{k-1}} \right) \Delta t \right] + Q_{k-1} \exp\left(j\omega t_k \right) \\
&= \left[A_{k-1} - Q_{k-1} \exp\left(j\omega t_{k-1} \right) \right] \exp\left[\left(j\omega_{r,k-1} - \frac{1}{\tau_{k-1}} \right) \Delta t \right] + Q_{k-1} \exp\left(j\omega t_k \right).
\end{aligned} \tag{11}
$$

These iterative equations can be implemented in Verilog-A as shown in Fig. 4. The input parameters for the model are the voltage applied to the PN junction (*vin*), wavelength of the incident optical field (*vlambda*), and clock signal that provides time-step for the calculation (*vclk*). At every rising edge of the clock signal, the transient response given as Eq. (11) is calculated with the corresponding optical parameters, *n_m*, *tl* and *te*, where each represents the ratio between η_{eff} and m, τ_l and τ_e, respectively. The parameter *r* is the radius of the ring. The period of the clock signal is the same as the time-step for the calculation, *dt*. The dependence of such optical parameters as *n_m, tl* and *te* on the input voltage should be experimentally determined. In our model, the dependence is modeled with a linear equation for *n_m* and a quadratic equation for *tl* and *te*, as will be described in in Section III.

```
// MRM_BEHAVIOUR, veriloga

`include "constants.vams"
`include "disciplines.vams"

module MRM_BEHAVIOUR (vin,vlambda,vclk,vout);

electrical      vin,vlambda,vclk,vout;
real            in,lambda,out;
real            Rq,Iq,Ra,Ia;
real            Ra_temp,Ia_temp;
real            Rout,Iout;
real            t,w,n_m,te,tl;

parameter real c=299792458;
parameter real pi=3.141592;
parameter real dt=200e-15;      // time-step
parameter real r=8e-6;          // radius of the ring

analog begin
@(cross(V(vclk), +1)) begin
in = V(vin);    lambda = V(vlambda); w = 2*pi*c/lambda;

// OPTICAL PARAMETERS
n_m = c1*in + c2;               // neff / m
te= c3*pow(in,2) + c4*in + c5;  // ring-bus coupling
tl=c7*pow(in,2)+c8*in+c9;       // round-trip loss
```

```
Ra_temp = Ra; Ia_temp = Ia;

Rq = (-1*sqrt(2/te))*(w-(1/n_m)*c/r)
     / (pow(1/te+1/tl,2)+pow(w-(1/n_m)*c/r,2));
Iq  = (1/te+1/tl)*(-1*sqrt(2/te))
     / (pow(1/te+1/tl,2)+pow(w-(1/n_m)*c/r,2));

Ra=exp(-1*(1/te+1/tl)*dt)
    *((Ra_temp-Rq*cos(w*t)+Iq*sin(w*t))*cos((1/n_m)*c/r*dt)
    -(Ia_temp-Iq*cos(w*t)-Rq*sin(w*t))*sin((1/n_m)*c/r*dt))
    +Rq*cos(w*(t+dt))-Iq*sin(w*(t+dt));

Ia=exp(-1*(1/te+1/tl)*dt)
    *((Ra_temp-Rq*cos(w*t)+Iq*sin(w*t))*sin((1/n_m)*c/r*dt)
    +(Ia_temp-Iq*cos(w*t)-Rq*sin(w*t))*cos((1/n_m)*c/r*dt))
    +Rq*sin(w*(t+dt))+Iq*cos(w*(t+dt));

Rout = cos(w*t) + sqrt(2/te)*Ia_temp;
Iout = sin(w*t) - sqrt(2/te)*Ra_temp;
out = pow(Rout,2)+pow(Iout,2);
t=t+dt;
end

V(vout) <+ out;
end
Endmodule
```

Fig. 4. Behavioral model in Verilog-A.

Since Verilog-A does not support complex numbers, variables for the real and the imaginary parts are separately defined and processed. *Ra* and *Ia*, *Ra_temp* and *Ia_temp*, and *Rq* and *Iq* are the real and imaginary parts for a_k, a_{k-1}, and Q_k, respectively. Exponential functions having imaginary numbers are converted into the sinusoidal functions.

#231700 - $15.00 USD Received 30 Dec 2014; revised 4 Mar 2015; accepted 18 Mar 2015; published 30 Mar 2015

3. Model verification

The Si MRM device used for verifying our behavior model is fabricated through OpSIS-IME multi-project wafer foundry service. Figures 5(a) and 5(b) show the microphotograph and the cross-section of the fabricated device. The radius of the ring waveguide is 8-μm and the nominal gap between ring and bus waveguides is 300-nm. It is implemented with 220-nm thick Si layer on 2-μm thick buried oxide layer. 500-nm wide rib waveguide is used for ring and bus waveguides. A lateral PN junction is formed in the ring waveguide except around the directional coupler. The nominal doping concentrations for the junction are 2 x 10^{18} /cm^3 for P region and 3 x 10^{18} /cm^3 for N region.

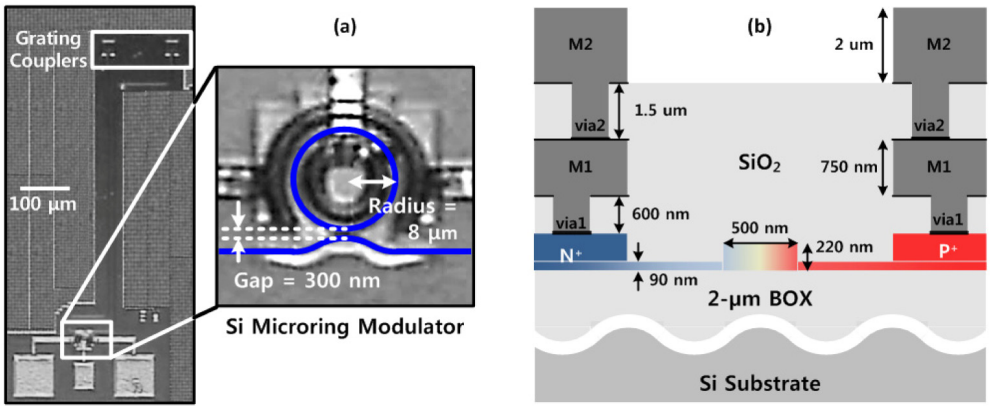

Fig. 5. (a) Microphotograph and (b) cross-section of fabricated Si MRM.

As the first step, numerical values of parameters used in our model have to be extracted from the fabricated Si MRM. Electrical model parameters are extracted by fitting simulated S_{11} coefficients of the equivalent circuit shown in Fig. 2 to measured S_{11}. Figures 6(a) and 6(b) show the magnitude and phase responses of measured (circles) and simulated by ADS (solid lines) S_{11}. The extracted numerical values of the electrical parameters are given in Table 1.

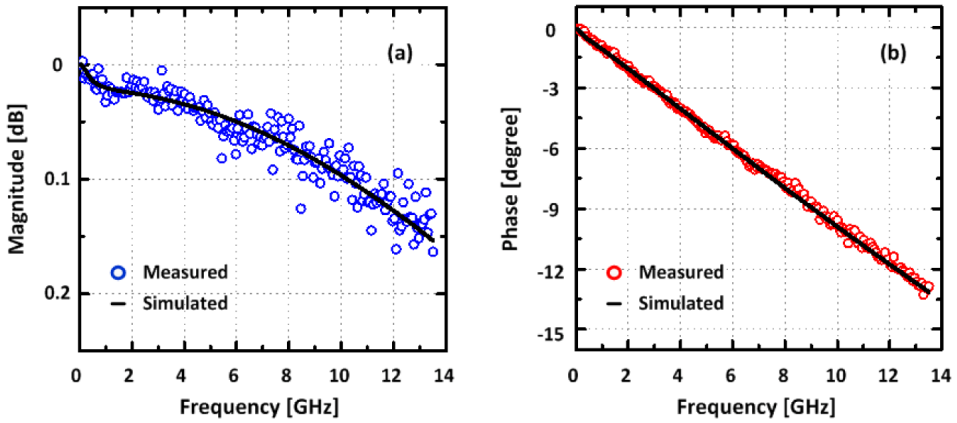

Fig. 6. Curve-fitting of the simulated S_{11} to the measurements: (a) Magnitude response (b) Phase response.

#231700 - $15.00 USD Received 30 Dec 2014; revised 4 Mar 2015; accepted 18 Mar 2015; published 30 Mar 2015

Table 1. Extracted parameter values of the Si MRM

Parameter	Description	Value
C_{PAD}	Parasitic capacitance of the signal pads	13.4 fF
R_{si}	Series resistance of the bulk Si	19.3 kΩ
C_{ox}	Capacitance through the oxide layer	21.3 fF
C_j	Depletion capacitance of the PN junction	14.7 fF
R_s	Series resistance of the PN junction	211 Ω

Optical model parameter values are extracted by fitting the measured optical power transmission characteristics of the Si MRM to the steady-state responses of our model obtained from Eq. (1) and Eq. (2) by letting $\frac{d}{dt}a(t) = j\omega a(t)$, or

$$\left|\frac{E_t}{E_i}\right|^2 = \left|\frac{j(\omega-\omega_r)+\frac{1}{\tau_l}-\frac{1}{\tau_e}}{j(\omega-\omega_r)+\frac{1}{\tau_l}+\frac{1}{\tau_e}}\right|^2. \quad (12)$$

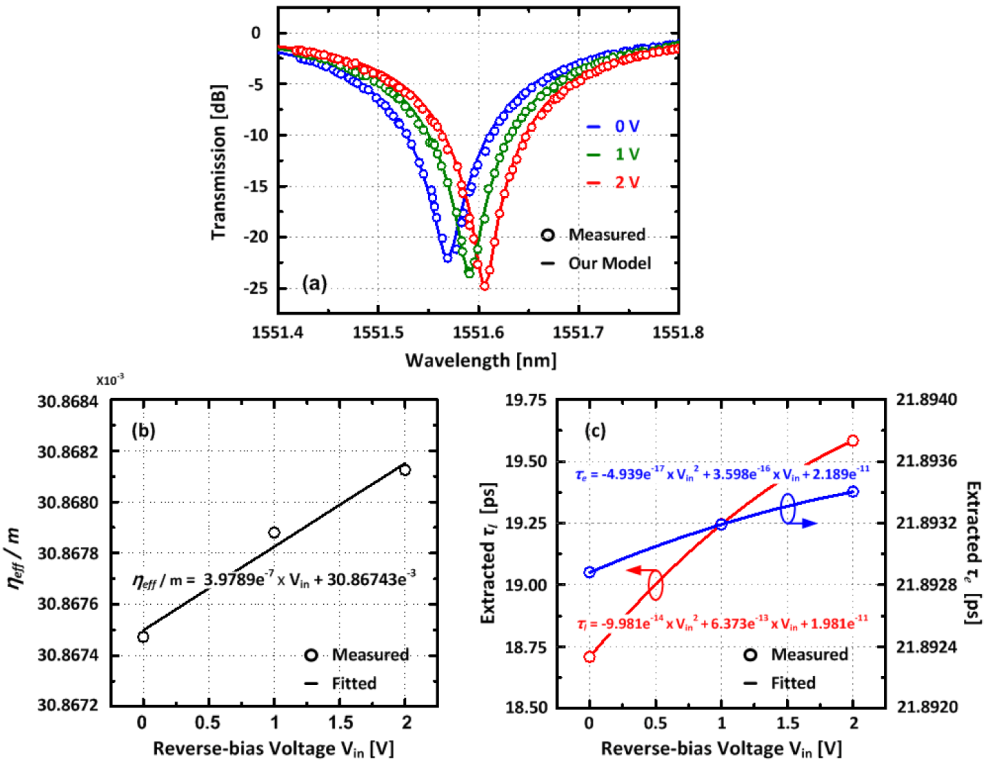

Fig. 7. (a) Measured and fitted optical transmission characteristics. (b) Extracted η_{eff} / m. (c) Extracted τ_l and τ_e.

Specifically, $\frac{\eta_{eff}}{m}$ is determined from the measured resonance wavelength using the resonance condition $m\lambda_{res} = \eta_{eff} L$, where λ_{res} represents the resonance wavelength. The values for τ_l and τ_e are determined with the minimum mean square error curve-fitting technique [17]. Parameter extraction is done for three different reverse bias voltages of 0, 1,

#231700 - $15.00 USD Received 30 Dec 2014; revised 4 Mar 2015; accepted 18 Mar 2015; published 30 Mar 2015

2V. The extracted values at each bias voltage are 0.0308674, 0.0308679, 0.0308682 for $\frac{\eta_{eff}}{m}$, 18.7081 ps, 19.2456 ps, 19.5853 ps for τ_l, and 21.8929 ps, 21.8932 ps, 21.8934 ps for τ_e. The voltage dependence of $\frac{\eta_{eff}}{m}$, τ_l and τ_e are approximated by a linear equation for $\frac{\eta_{eff}}{m}$, and quadratic equations for τ_l and τ_e as shown in Figs. 7(b) and 7(c).

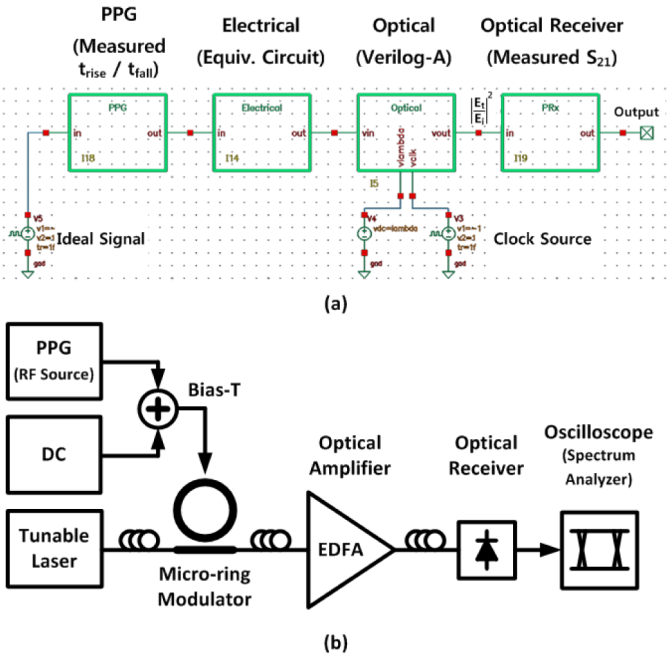

Fig. 8. (a) Simulation setup. (b) Measurement setup.

Using our model with the extracted parameters, the Si MRM dynamic characteristics can be easily simulated with Spectre in Cadence, one of the most widely-used CAD tools for electronic circuit design. Figure 8(a) shows the schematic used for such simulation. As mentioned before, a clock signal is used for in providing the time-step for model simulation.

In order to confirm the accuracy of our model, the simulation results for the Si MRM transient responses are compared with the measurement results. The measurement setup is shown in Fig. 8(b). The tunable laser source provides the light into the Si MRM through a grating coupler. The PPG provides the electrical signals to the modulator with the desired DC offset voltage. In order to avoid any self-heating of the Si MRM [18], the optical power injected into the Si MRM is minimized during measurement. With −5-dBm injection into the grating coupler and about 5-dB coupling loss, the optical power level inside the waveguide is about −10-dBm. This requires amplification of output optical signal with an erbium-doped fiber amplifier. The optical receiver converts the optical output into the electrical signals, which are observed with an oscilloscope.

For accurate comparison between simulation and measurement results, the measurement condition should be accurately accounted for. For this, rising and falling times of electric signals provided by the PPG as well as the frequency response of the optical receiver used in measurement are measured and their equivalent circuits are used in simulation. The influence of the optical amplifier is not considered in our simulation since it does not influence the dynamics of our measurement.

#231700 - $15.00 USD Received 30 Dec 2014; revised 4 Mar 2015; accepted 18 Mar 2015; published 30 Mar 2015

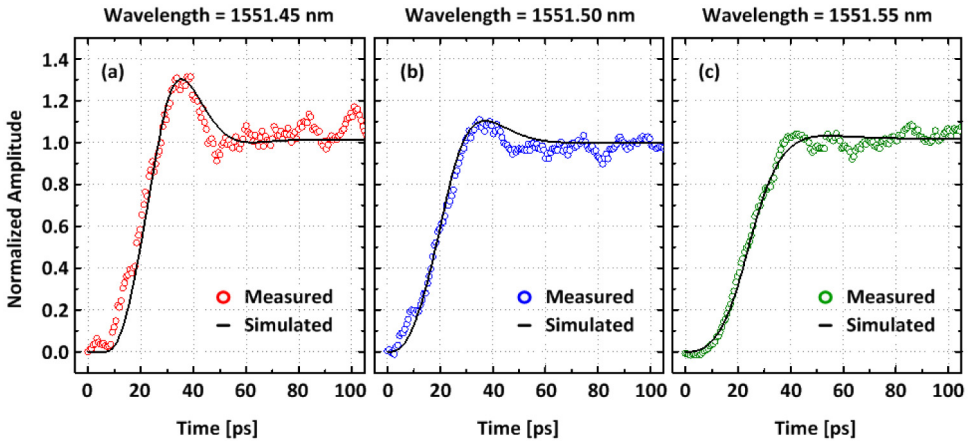

Fig. 9. Measured and simulated step response at the wavelength of (a) 1551.45 nm (b) 1551.50 nm (c) 1551.55 nm.

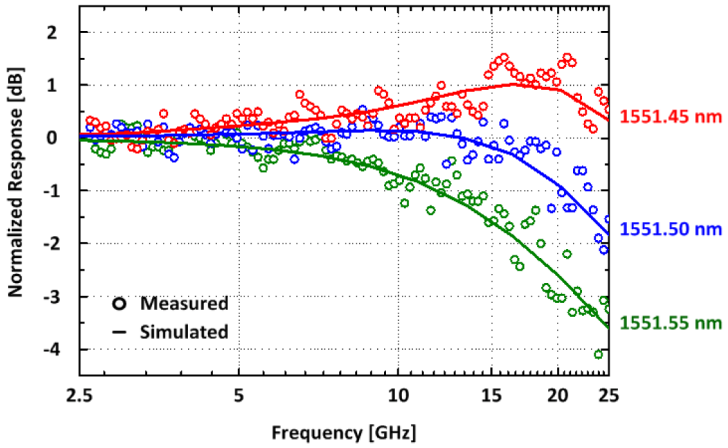

Fig. 10. Measured and simulated frequency response at the wavelength of 1551.45 nm, 1551.50 nm, and 1551.55 nm.

Figures 9(a), 9(b) and 9(c) show the measured and simulated step responses of the Si MRM at three different input wavelengths of 1551.45 nm, 1551.50 nm, and 1551.55 nm, respectively. The resonance wavelength of Si MRM at 0V bias is 1551.565 nm as can be seen in Fig. 7(a). For this measurement, a voltage step from 0V to 2V is applied to Si MRM by the PPG. A time step of 200-fs is used for simulation. Different amounts of peaking are observed for Si MRMs at different wavelengths, which is due to the wavelength-dependent frequency response of the Si MRM [19–21]. Figure 10 shows the normalized modulation frequency responses measured at three different wavelengths as well as the simulated results with our model. For this measurement, an RF source is used instead of PPG as an input, and the output signals are observed with a spectrum analyzer. When the separation between input and resonance wavelengths is larger, the MRM has a peaking at higher frequency, which results in the larger overshoot for the step response. As can be seen in the figures, our behavioral model accurately describes such wavelength-dependent step and frequency responses.

#231700 - $15.00 USD Received 30 Dec 2014; revised 4 Mar 2015; accepted 18 Mar 2015; published 30 Mar 2015

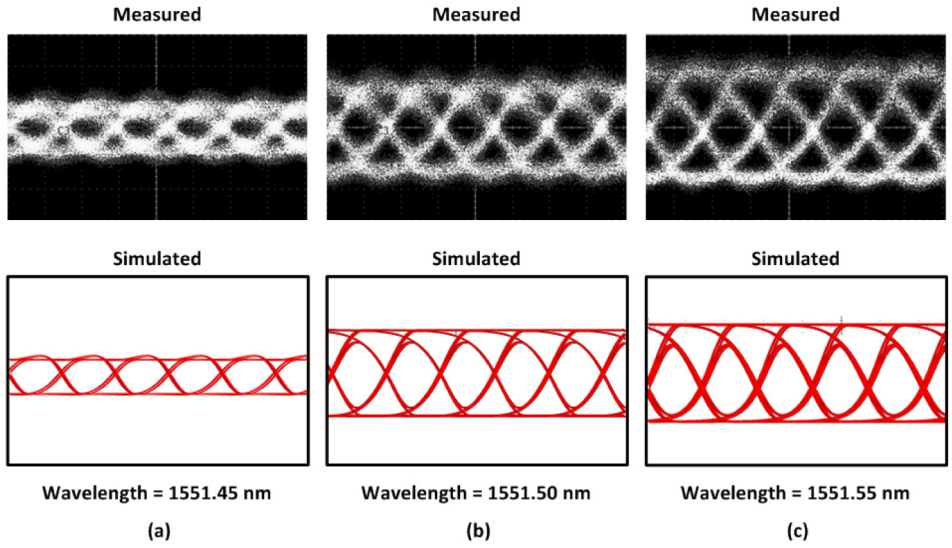

Fig. 11. Measured and simulated eye-diagrams for 28-Gb/s PRBS 2^{31}-1 pattern at the wavelength of (a) 1551.45 nm (b) 1551.50 nm (c) 1551.55 nm.

For further verification, simulated and measured eye diagrams are compared for 28-Gb/s 2^{31}-1 PRBS data. For obtaining simulated eye diagrams, first 40 bits before the Si MRM reaches the steady-state are discarded. Similar to the step responses, we observe the wavelength dependent eye diagrams as shown in Figs. 11(a), 11(b) and 11(c). The maximum on-off ratio is observed for at λ = 1551.55 nm, but the maximum eye opening is observed at λ = 1551.5 nm, where the SI MRM has larger modulation bandwidth. With our model, which can accurately describe the wavelength-dependent Si MRM dynamics, we can take the Si MRM as one of the easily accessible function blocks in the design environment and use it along with other electronic blocks for realizing optimally-performing optical transmitters for various optical interconnect applications.

4. Conclusion

We developed an accurate behavioral model for the Si MRM in Verilog-A. The accuracy of our model was experimentally verified with a fabricated Si MRM device. In addition, we provided the parameter extraction technique, whose accuracy is extremely important for any device model, and details of the numerical calculation process. Our approach of implementing the Si MRM model in Verilog-A is highly valuable as it allows accurate simulation of the Si MRM in the well-established electronic design environment. We believe such compatibility is very important for successful realization of Si photonic devices integrated with Si electronic circuits.

Acknowledgments

This work was supported by the National Research Foundation of Korea funded by the Korean Government (MEST) under Grant 2012R1A2A1A01009233.

#231700 - $15.00 USD Received 30 Dec 2014; revised 4 Mar 2015; accepted 18 Mar 2015; published 30 Mar 2015